Theoretical Analysis of the Mechanism of Cationic Pd(II)-catalyzed Fujiwara-Moritani Reaction①

REN Ying② WANG Tao ZHANG Ting-Ting
JIA Jian-Feng WU Hai-Shun
(*Key Laboratory of Magnetic Molecules and Magnetic Information Materials of Ministry of Education, School of Chemistry and Materials Science, Shanxi Normal University, Linfen* 041000, *China*)

ABSTRACT A systematic theoretical investigation has been studied on Fujiwara-Moritani reaction between 3-methoxyacetanilide with *n*-butyl acrylate by means of density functional theory (DFT) calculations when two types of Pd(II) catalysts are employed. In $[Pd(MeCN)_4](BF_4)_2$ catalytic cycle, a 1,4-benzoquinone(BQ)-induced C−H activation of *trans*-$(MeCN)_2Pd(BQ)^{2+}$ with 3-methoxyacetanilide occurs as the first step to give **DC-4$_{MeCN}$**, facilitating the insertion of *n*-butyl acrylate and *β*-hydride elimination, followed by recycling of catalyst through hydrogen abstraction of monocationic BQ fragment. In $Pd(OAc)_2$ catalytic cycle, it is proposed that the most favored reaction pathway should proceed in dicationic mechanism involving a BQ-assisted hydrogen transfer for C−H activation by Pd active catalyst $(HOAc)_2Pd(BQ)^{2+}$ to generate **DC-4$_{HOAc}$**, promoting acrylate insertion and *β*-hydride elimination, followed by the regeneration of catalyst to give the final product. The calculations indicate that the rate-determining step in $[Pd(MeCN)_4](BF_4)_2$ catalytic system is the acrylate insertion, while it is the regeneration of catalyst in the $Pd(OAc)_2$ catalytic system. In particular, the roles of BQ and ligand effects have also been investigated.

Keywords: C−H bond activation, DFT studies, Pd(II) catalyst, reaction mechanism;
DOI: 10.14102/j.cnki.0254–5861.2011–3077

1 INTRODUCTION

Transition-metal-catalyzed C−H activation has emerged as the most important and useful means to form C−C, C−O, C−N, and C−X (X = Cl, Br, I) bonds in modern organic synthesis chemistry[1]. Compared with the traditional catalytic reactions where expensive unstable organometallic reagents are often required and the poor atom economy is resulted, the direct C−H bond activation has been well developed and improved, thus providing a sustainable and efficient strategy to synthesize diverse organic molecules from simple hydrocarbon derivatives[2-5].

Among the various transition-metal-catalyzed cross coupling reactions[6], palladium(II) catalysts exhibited excellent catalytic activity in C−H activation reactions[7]. The Fujiwara-Moritani (FM) reaction is one typical of such Pd-catalyzed C−C coupling reactions, first reported in 1967[8]. However, Many efforts on FM reaction have been often limited by the high temperature, anhydrous acidic environments, and high pressures[9]. Commonly, FM reactions should be carried out in the presence of external acid. Mulligan et al. reported Pd-catalyzed FM reaction of *p*-methylacetanilide with *n*-butyl acrylate in the presence of toluenesulfonic acid and BQ[10]. Danton et al. reported site-selective Pd-catalyzed FM reaction of N,S-heterocyclic systems with olefins in PivOH[11]. Typically, some acids such as HOAc, TFA, and PTSA have been used to promote these C−H activation reactions[12]. Recently, Nishikata and Lipshutz have reported a novel Pd(II)-catalyzed FM reaction of 3-methoxyacetanilide with *n*-butyl acrylate to produce electron-rich cinnamates (Scheme 1a)[13]. More interestingly, this reaction carries out not only at room temperature in water as the only medium, but most notably without the addition of external acids.

The Pd-catalyzed C−H activation reactions have been extensively studied both experimentally and theoretically[14], which are devoted to understanding the mechanisms involved

Received 25 December 2020; accepted 8 April 2021
① This work was supported by the Natural Science Foundations of China (21501115)
② Corresponding author. E-mail: ren.ying1991@163.com

in the cleavage of C−H bond and the role of catalytic species. Especially, $Pd(OAc)_2$ as catalyst is oftentimes used, where acetate is considered to be involved in aromatic proton-abstraction[15]. Thus, the role of $Pd(OAc)_2$ is generally to activate the arene and abstract the hydrogen atom of the C−H bond by one of the acetate ligands in a classic six-membered transition state (Scheme 2). Nishikata's reaction represented a highly active dicationic Pd(II) catalyst, $[Pd(MeCN)_4](BF_4)_2$, which can easily activate aromatic C−H bonds without acetate ligands and external acids (Scheme 1a). However, it was found that the acid plays an important role in the reaction catalyzed of $Pd(OAc)_2$ (Scheme 1b). On the basis of the results, they also proposed the cationic Pd(II)-catalyzed mechanism of FM reactions, shown in Scheme 3, which involves a Pd(II)/Pd(0) redox cycle mechanism. Initially, the aromatic C−H bond activation between 3-methoxyacetanilide with the cationic Pd(II) species proceeds using the directing group via Wheland-like species to give monocationic species, followed by alkyne insertion. The *β*-hydride elimination and regeneration catalyst take place to form the final product. Nevertheless, BQ was found to be critical to the two Pd(II) catalytic systems, without which the reaction essentially did not take place in water.

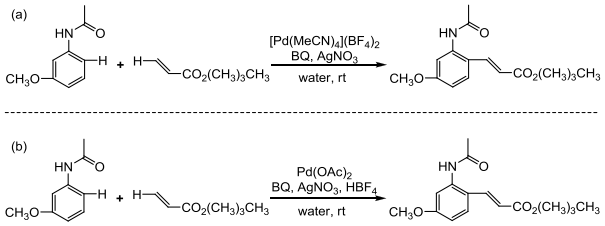

Scheme 1. Pd(II)-catalyzed C−H activation/C−C cross-coupling reaction of a 3-methoxyacetanilide and a *n*-butyl acrylate

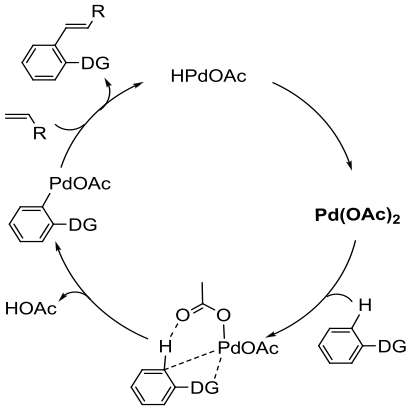

Scheme 2. General mechanism of $Pd(OAc)_2$ catalyzed C−H activation reactions

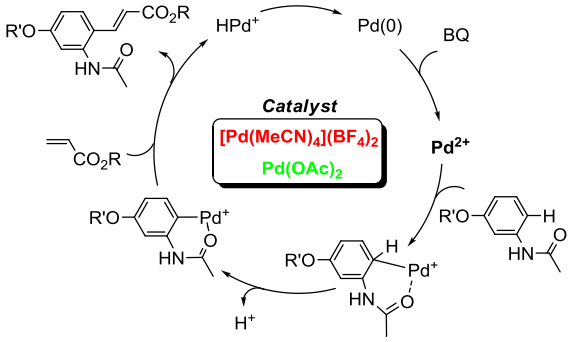

Scheme 3. Mechanism proposed by Nishikata and coworkers

In view of the importance and versatility of C−C cross-coupling reactions via direct C−H activation, it is necessary to develop mechanistic understanding of Nishikata's FM reaction. In this paper, with the aid of DFT calculations, we have investigated the mechanism of Pd(II)-catalyzed C−C coupling reaction of 3-methoxyacetanilide with *n*-butyl

acrylate in detail. Through these studies, we hope to answer the following questions: (1) How does the cationic palladium species $[Pd(MeCN)_4](BF_4)_2$ catalyze the reaction without acetate ligands? (2) Does the BQ promote the catalytic cycle? If yes, how does the BQ play its role in catalytic cycle? (3) Why acid was found to be vital to the $Pd(OAc)_2$ catalytic systems? These questions are very important for us to understand the reaction better and may provide helpful information for the development of new, more effective catalyst systems on similar reactions.

2 COMPUTATIONAL DETAILS

All the energies and molecular geometries presented in this paper were performed with the Gaussian 09[16] program package, using the B3LYP level of density functional theory (DFT)[17-19]. Vibrational frequency was calculated at the same level of theory to ensure each equilibrium structure with no imaginary frequency or each transition state with only one imaginary frequency and to get thermal energy corrections and zero-point energy (ZPE). Especially, the only one imaginary frequency of every transition state showed the desired vibration orientation. The 6-311++G(*d*, *p*)[20] basis set was used to describe C, H, O, and N atoms, while the Pd atom was described using the LANL2DZ[21] basis set. Polarization function was added for Pd (ζ_f = 1.472)[22]. Furthermore, intrinsic reaction coordinates (IRC)[23] were also calculated for the transition states to identify that such structures are connecting the two adjacent minima on the potential energy surface. In order for further explanation, the natural bond orbital (NBO)[24] package was used for some structures to analyze the natural charges.

To examine the aforementioned method reliability, the M06[25]/SDD[26] was employed and single-point energy calculations for the structures involved in the whole reaction were carried out. Compared with the relative energies calculated by the two density functionals B3LYP and M06, it is found that the general trends of the potential energy surface are consistent with each other (see Table S1 in the Supporting Information). In addition, the SMD continuum solvation model[27] in water was used to account for the solvent effects. The solvation Gibbs energy was performed at the B3LYP/6-311++G(*d*, *p*) (LANL2DZ for Pd atom) level and added to the gas-phase thermal correction Gibbs energy to get the solvent-corrected Gibbs energy.

3 RESULTS AND DISCUSSION

To understand the detailed mechanism of Pd-catalyzed FM reaction of 3-methoxyacetanilide with *n*-butyl acrylate, the two catalytic systems of $[Pd(MeCN)_4](BF_4)_2$ and $Pd(OAc)_2$ have been comprehensively investigated by discussing series of reasonable structures of intermediates and transition states. Subsequently, a comparison of two catalytic cycles $[Pd(MeCN)_4](BF_4)_2$ and $Pd(OAc)_2$ is studied.

3. 1 Mechanism of $[Pd(MeCN)_4](BF_4)_2$ catalyzed C−H activation/C−C cross-coupling reaction

The mechanism of $[Pd(MeCN)_4](BF_4)_2$ catalyzed FM reaction is proposed on the basis of Nishikatas' study. There are four steps in the cycle: C−H activation, acrylate insertion, *β*-hydride elimination, and recycling of catalyst. The Gibbs energy profiles for this mechanism are shown in Figs. 1, 3, and 5, and some critical geometrical structures of proposed pathways are illustrated in Figs. 2 and 4.

This mechanism starts with *trans*-$(MeCN)_2Pd(BQ)^{2+}$ (**DC-0$_{MeCN}$**). The complex is chosen as the starting point for the following reasons: (1) Nishikata and Lipshutz reported the catalyst is a dicationic palladium(II) species, which is formed by ionization of the catalyst precursor $[Pd(MeCN)_4](BF_4)_2$ in water. And BQ could competitively ligate the palladium(II) catalyst. More importantly, BQ presumably participates in proton abstraction. (2) Four possible active forms of catalyst from $[Pd(MeCN)_4](BF_4)_2$ are calculated (Scheme 4). It is found that *trans*-$(MeCN)_2Pd(BQ)^{2+}$ is more stable than *trans*-$(BQ)_2Pd(MeCN)^{2+}$ and *cis*-$(BQ)_2Pd(MeCN)^{2+}$ by 0.8 and 2.3 kcal/mol, whereas *cis*-$(MeCN)_2Pd(BQ)^{2+}$ is more stable than *trans*-$(MeCN)_2Pd(BQ)^{2+}$ by 2.5 kcal/mol, respectively. It is noteworthy that the structure of *cis*-$(MeCN)_2Pd(BQ)^{2+}$ is not suitable for C−H activation. From the geometric configuration of *cis*-$(MeCN)_2Pd(BQ)^{2+}$, it can be seen that as the Pd center activates the ortho carbon of directing group, the abruption of BQ is concomitant. The subsequent C−H activation fails because hydrogen transfer cannot occur without the base ligand. Thus, the *trans*-$(MeCN)_2Pd(BQ)^{2+}$ is more likely to be the active species to bind the reactant-catalyst coordination site through the abruption of a MeCN ligand, contributing to the later C−H activation with the help of BQ molecule. Apart from the lower energy, the geometric configuration is another crucial factor for choosing *trans*-$(MeCN)_2Pd(BQ)^{2+}$ as the active catalyst species and also as the energy reference together with the reactants.

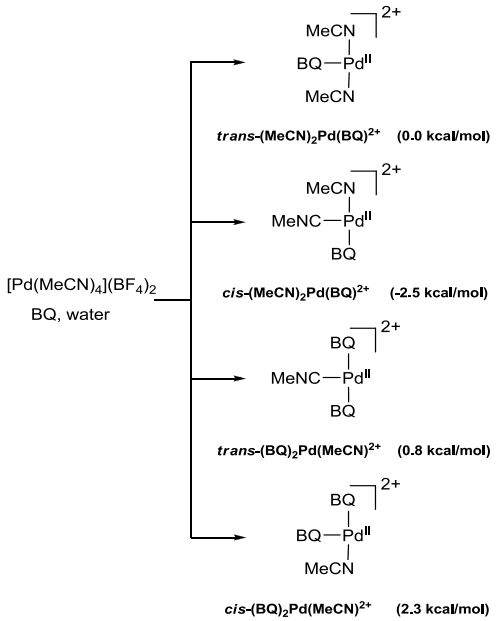

Scheme 4. Forms of the catalyst from $[Pd(MeCN)_4](BF_4)_2$

C−H activation begins with coordination of 3-methoxyacetanilide and **DC-0$_{MeCN}$** relaxing to the intermediate **DC-1$_{MeCN}$**, followed by releasing one molecule MeCN ligand from the Pd center. Then, the vacant coordination site would be occupied by the C−H bond of 3-methoxyacetanilide via the transition state **DC-TS(2/3)$_{MeCN}$**. The intermediate **DC-3$_{MeCN}$** formed is feathered by an agnostic interaction of C−H bond to Pd atom. Following this, the BQ-induced hydrogen transfer proceeds in an *σ*-bond metathesis mechanism resulted in the cleavage of the C−H bond, as shown in Fig. 1. The feature of dicationic transition state **DC-TS(3/4)$_{MeCN}$** is an intermolecular hydrogen transfer of the H3 atom from 3-methoxyacetanilide to the O2 atom of BQ ligand, concomitant with a ruptured Pd−O_{BQ} bond (3.243 Å) and C−H bond (1.391 Å), leading to the charge separation between the more stable monocationic intermediate **DC-4$_{MeCN}$** and the monocationic BQ fragment (4-oxocyclohexa-2,5-dienylidene)oxonium. The Gibbs energy profile in Fig. 1 shows that the C−H activation section is predicted to be exoergic by 10.3 kcal/mol with a moderate Gibbs energy barrier of 23.8 kcal/mol. From the above-mentioned relative Gibbs energies, in order to test the activity of *trans*-$(BQ)_2Pd(MeCN)^{2+}$ and *cis*-$(BQ)_2Pd(MeCN)^{2+}$, the corresponding C−H activations have been also calculated. Such *trans*-$(BQ)_2Pd(MeCN)^{2+}$ and *cis*-$(BQ)_2Pd(MeCN)^{2+}$ catalyzed C−H activation pathways are not favorable both kinetically and thermodynamically with respect to the *trans*-$(MeCN)_2Pd(BQ)^{2+}$. The relative information is detailed in the Supporting Information.

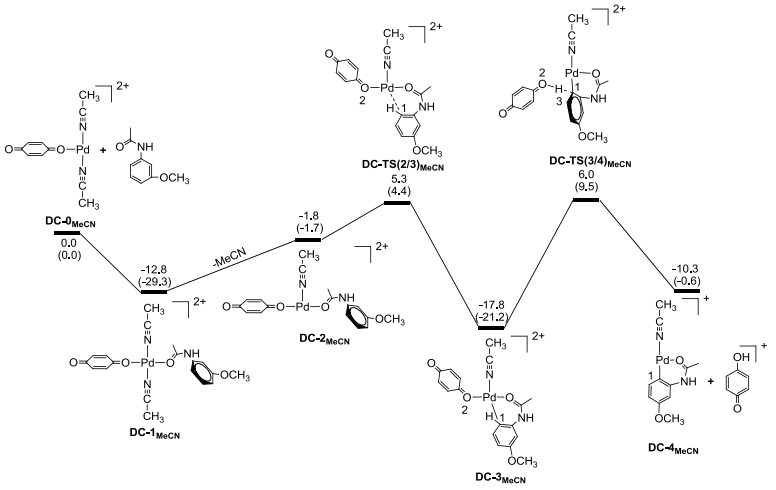

Fig. 1. Geometrical structures and Gibbs energy profile for the C−H activation in $[Pd(MeCN)_4](BF_4)_2$. The solvation-corrected relative Gibbs energies and electronic energies (in parentheses) are given in kcal/mol

Based on the generation of the intermediate **DC-4$_{MeCN}$**, we studied the acrylate insertion and *β*-hydride elimination of Pd-catalyzed with MeCN ligand. The T-shaped three-coordinate intermediate **DC-4$_{MeCN}$** with a vacant site is coordinated by the C=C double bond of acrylate, leading to the four-coordinate intermediate **DC-5a$_{MeCN}$**. Then the C4 atom of acrylate attacks the C1 atom of 3-methoxyacetanilide, which results in the formation of C−C bond through a four-membered cyclic transition state **DC-TS(5a/6a)$_{MeCN}$**. The Gibbs energy barrier for this step is 16.9 kcal/mol. In **DC-6a$_{MeCN}$**, the O atom of substrate *n*-butyl acrylate coordinates with Pd and the coordination mode of the C=C double bond changes from $\eta^2 \rightarrow \eta^1$ to Pd, which guarantees the stability of **DC-6a$_{MeCN}$** effectively. Next, **DC-6a$_{MeCN}$** undergoes *β*-hydride migration to regenerate alkene and get (η^2-alkenyl)Pd intermediate **DC-7a$_{MeCN}$** via a five-coordinate transition state **DC-TS(6a/7a)$_{MeCN}$**. Furthermore, the acrylate insertion and *β*-hydride elimination of Pd-catalyzed without ligand or with BQ as ligand are also studied, as shown in Fig. 2. For simplification, Fig. 3 only shows the Gibbs energy profile of favorite path, and other paths are given in the supporting information (Fig. S3). By comparing the energetics of these pathways shown above, it is illustrated that the pathway with MeCN ligand is preferred, because the Gibbs energy barrier of the C−C bond coupling portion (**DC-5a$_{MeCN}$** → **DC-6a$_{MeCN}$**, **DC-6b$_{MeCN}$** → **DC-7b$_{MeCN}$**, and **DC-5c$_{MeCN}$** → **DC-6c$_{MeCN}$**) is the lowest Gibbs energy maximum for the three paths (19.7, 28.0, and 25.6 kcal/mol relative to **DC-4$_{MeCN}$**, respectively). The corresponding transition states, **DC-TS(5a/6a)$_{MeCN}$** and **DC-TS(5c/6c)$_{MeCN}$**, are lower in energy than **DC-TS(6b/7b)$_{MeCN}$** mainly due to the ligand effects. Furthermore, the weaker metal coordination of MeCN ligand versus BQ ligand leads to **DC-TS(5a/6a)$_{MeCN}$** having more activity, as revealed by the charges of the Pd and N atoms (0.469 *e* and –0.383 *e*) versus the Pd and O atoms in **DC-TS(5c/6c)$_{MeCN}$** (0.507 *e* and –0.547 *e*). Frontier molecular orbital (FMO) calculations are performed to support the above claim (Fig. S7). The data imply that the MeCN ligand gives low activation barrier as compared to those with BQ ligand or without ligand.

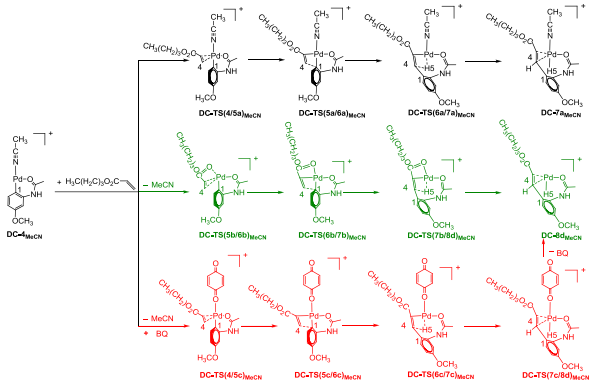

Fig. 2. Proposed pathways for acrylate insertion and *β*-hydride elimination from DC-4$_{MeCN}$

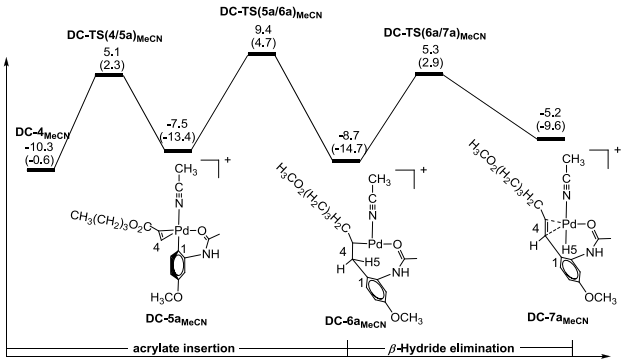

Fig. 3. Gibbs energy profile for acrylate insertion and *β*-hydride elimination from DC-4$_{MeCN}$ to DC-7a$_{MeCN}$ in [Pd(MeCN)$_4$](BF$_4$)$_2$. The solvation-corrected relative Gibbs energies and electronic energies (in parentheses) are given in kcal/mol

Following the *β*-hydride elimination, the regeneration of catalyst takes place. From **DC-7a$_{MeCN}$**, four pathways can be conceivable, as shown in Fig. 4. Fig. 5 only shows the Gibbs energy profile of the favorite path, and other paths are given

in supporting information (Fig. S4). Replacement of the product ligand in complex **DC-7a$_{MeCN}$** by MeCN ligand or BQ ligand would give precursor complexes **DC-8a$_{MeCN}$**, **DC-8b$_{MeCN}$**, and **DC-8c$_{MeCN}$**, respectively. **DC-8d$_{MeCN}$** having the coupling product as a ligand is relatively more unstable than **DC-7a$_{MeCN}$** by 13.3 kcal/mol. On the basis of the conformation of complexes **DC-8a$_{MeCN}$**, **DC-8b$_{MeCN}$**, **DC-8c$_{MeCN}$**, and **DC-8d$_{MeCN}$**, the incoming monocationic BQ fragment would enter the Pd coordination sphere by attacking the vacant site. These lead to the four-coordination complexes **DC-9a$_{MeCN}$**, **DC-9b$_{MeCN}$**, **DC-9c$_{MeCN}$**, and **DC-9d$_{MeCN}$** correspondingly. Furthermore, four corresponding transition states **DC-TS(8a/9a)$_{MeCN}$**, **DC-TS(8b/9b)$_{MeCN}$**, **DC-TS(8c/9c)$_{MeCN}$**, and **DC-TS(8d/9d)$_{MeCN}$** have been located. As illustrated in Fig. 5, the step (**DC-8a$_{MeCN}$** → **DC-9a$_{MeCN}$**) needs to overcome the Gibbs energy barrier of 11.9 kcal/mol relative to **DC-7a$_{MeCN}$**, which is lower than the other steps (**DC-8b$_{MeCN}$** → **DC-9b$_{MeCN}$**, **DC-8c$_{MeCN}$** → **DC-9c$_{MeCN}$**, and **DC-8d$_{MeCN}$** → **DC-9d$_{MeCN}$**) shown in supporting information (Fig. S4) by 5.2, 13.6, and 9.9 kcal/mol in turn. The next step is the migration of H5 atom of **DC-9a$_{MeCN}$**, **DC-9b$_{MeCN}$**, **DC-9c$_{MeCN}$**, and **DC-9d$_{MeCN}$** to form the more stable conformations **DC-10a$_{MeCN}$**, **DC-10b$_{MeCN}$**, **DC-10c$_{MeCN}$**, and **DC-10d$_{MeCN}$**. The hydride migration transition states **DC-TS(9b/10b)$_{MeCN}$**, **DC-TS(9c/10c)$_{MeCN}$**, and **DC-TS(9d/10d$_{MeCN}$)** are clearly higher in energy than **DC-TS(9a/10a)$_{MeCN}$** relative to **DC-9a$_{MeCN}$**. Finally, the resulting **DC-10a$_{MeCN}$**, **DC-10b$_{MeCN}$**, **DC-10c$_{MeCN}$**, and **DC-10d$_{MeCN}$** are then coordinated by BQ or MeCN ligand to regenerate the active **DC-0$_{MeCN}$**, respectively. All these results indicate that the relative stability of these precursor complexes is closely related to the ligand. The complexes of the Pd center with two MeCN ligands are more active than those of the complexes of the Pd center (where L = MeCN, BQ, and product). Thus, the regeneration of catalyst via the pathway from **DC-8a$_{MeCN}$** to product is kinetically and thermodynamically favored over the regeneration of catalyst via the pathways from **DC8b$_{MeCN}$**, **DC8c$_{MeCN}$**, and **DC-8d$_{MeCN}$** to the product.

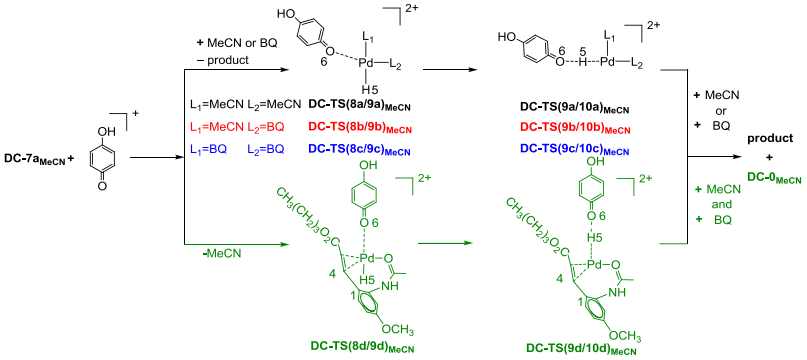

Fig. 4. Proposed pathways for regeneration of catalyst from DC-7a$_{MeCN}$

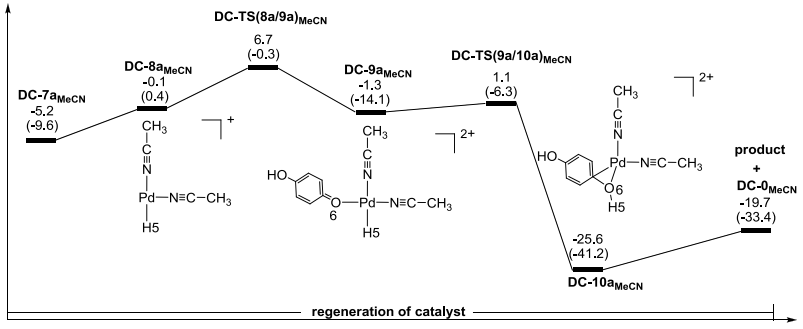

Fig. 5. Gibbs energy profile for regeneration of catalyst (DC-7a$_{MeCN}$ → DC-0$_{MeCN}$) in [Pd(MeCN)$_4$](BF$_4$)$_2$. The solvation-corrected relative Gibbs energies and electronic energies (in parentheses) are given in kcal/mol

On the basis of the above discussions, a whole catalytic cycle for the mechanism of [Pd(MeCN)$_4$](BF$_4$)$_2$ catalyzed FM reaction is completed. As shown in Figs. 1, 3, and 5, the compounds involved in the reaction coordinates of the most favorable pathway in kinetics and thermodynamics all have MeCN ligand. Obviously, the acrylate insertion is the rate-determining step of the catalytic cycle. The magnitude of the overall activation barrier (27.2 kcal/mol) is moderate,

demonstrating the feasibility of the proposed mechanism. Although the MeCN ligand is more catalytically active than the BQ ligand including stabilizing the dicationic palladium(II) species, the BQ is critical in the reaction inducing the proton migration in C−H activation and helping catalyst recovery.

3. 2 Mechanism of $Pd(OAc)_2$ catalyzed C−H activation/C−C cross-coupling reaction

For comparison, we also studied the C−H activation/C−C cross-coupling reaction catalyzed by $Pd(OAc)_2$. Two active forms of the Pd(II) catalysts, $(HOAc)Pd(BQ)_2^{2+}$ and $(HOAc)_2Pd(BQ)^{2+}$), could exist in the presence of HBF_4, BQ, and water. $(HOAc)_2Pd(BQ)^{2+}$ is more stable than $(HOAc)Pd(BQ)_2^{2+}$ by 1.7 kcal/mol. Therefore, the following discussion focuses on $(HOAc)_2Pd(BQ)^{2+}$ as the active catalyst. Detailed mechanism regarding how dicationic Pd catalyst $(HOAc)_2Pd(BQ)^{2+}$ (**DC-0$_{HOAc}$**) reacts with 3-methoxyacetanilide and *n*-butyl acrylate is given in this section.

As stated above, the first section of the catalytic reaction is proposed to be the C−H activation. Some geometrical structures and the Gibbs energy profile are given in Fig. 6. **DC-0$_{HOAc}$** coordinates with the 3-methoxyacetanilide to form intermediate **DC-1$_{HOAc}$**. Then a HOAc ligand leaves the Pd center, freeing space for the approach of the C1 atom, thus leading to intermediate **DC-2$_{HOAc}$** from which the Pd center coordinates with the C−H bond to cause the pre-activation of C−H bond via the corresponding transition state **DC-TS(2/3)$_{HOAc}$**. This gives intermediate **DC-3$_{HOAc}$**, featuring an agnostic interaction between C−H bond and the Pd center. The following step is C−H activation. This step occurs through *σ*-bond metathesis mechanism with a four-membered ring transition state **DC-TS(3/4)$_{HOAc}$**, in which the BQ-induced hydrogen transfer results in the cleavage of C−H bond. In **DC-TS(3/4)$_{HOAc}$**, the C−H bond is significantly lengthened relative to that in **DC-2$_{HOAc}$** (1.093 *vs* 1.390 Å), which implies that the interaction between C and H atoms begins to weaken. Simultaneously, the monocationic BQ moiety is easily ruptured from intermediate **DC-3$_{HOAc}$** to give monocationic intermediate **DC-4$_{HOAc}$**. The Gibbs energy barrier for the C−H activation going through **DC-TS(3/4)$_{HOAc}$** is calculated to be 21.0 kcal/mol.

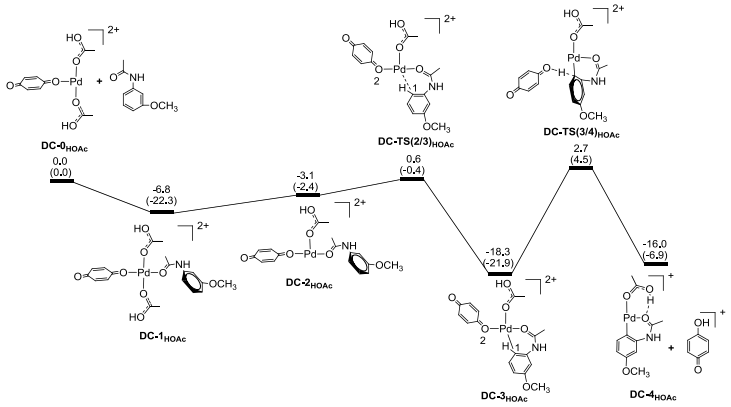

Fig. 6. Geometrical structures and Gibbs energy profile for the C−H activation in $Pd(OAc)_2$. The solvation-corrected relative Gibbs energies and electronic energies (in parentheses) are given in kcal/mol

In alkene insertion and *β*-hydride elimination, intermediate **DC-4$_{HOAc}$** reacts directly with *n*-butyl acrylate. The C=C double bond in *n*-butyl acrylate coordinates with the Pd center of **DC-4$_{HOAc}$** via transition state **DC-TS(4/5a)$_{HOAc}$** to form intermediate **DC-5a$_{HOAc}$**. Then the C4 atom of C=C double bond attacks C1 atom of the 3-methoxyacetanilide, giving the cross-coupling intermediate **DC-6a$_{HOAc}$** with a barrier of 19.1 kcal/mol. Subsequently, *β*-hydride elimination takes place via transition state **DC-TS(6a/7a)$_{HOAc}$**. The Gibbs energy profile in Fig. 8 shows that the section (**DC-4$_{HOAc}$** → **DC-7a$_{HOAc}$**) needs to overcome the low energy barrier of 21.4 kcal/mol. Furthermore, the monocationic Pd catalyst can also have two similar pathways including the presence of BQ ligand and the absence of ligand (Fig. 7), which are the same as what we found for the mechanism of $[Pd(MeCN)_4](BF_4)_2$ catalyzed reaction. The corresponding Gibbs energy barriers in the presence of BQ ligand and in the absence of ligand pathways are calculated to be 27.3 and 24.8 kcal/mol, respectively (Fig. S5). These results indicate that the section (**DC-4$_{HOAc}$** → **DC-7a$_{HOAc}$**) will react preferentially with *n*-butyl acrylate over other pathways.

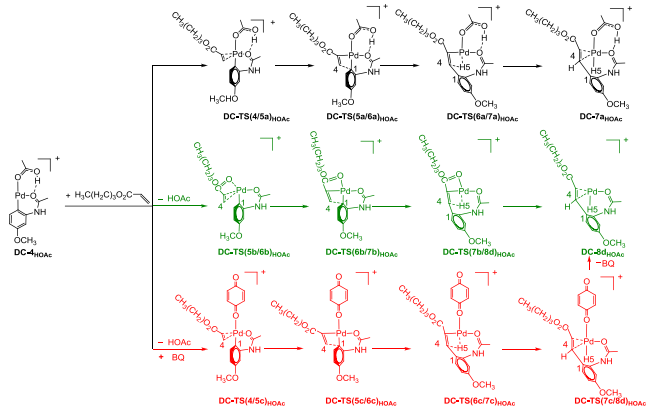

Fig. 7. Proposed pathways for acrylate insertion and *β*-hydride elimination from DC-4$_{HOAc}$

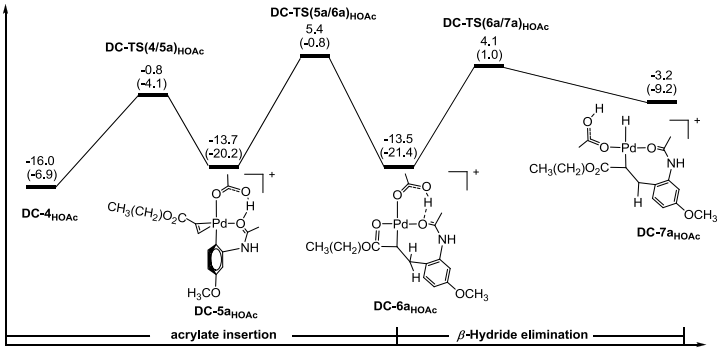

Fig. 8. Gibbs energy profile for acrylate insertion and *β*-hydride elimination from DC-4$_{HOAc}$ to DC-7a$_{HOAc}$ in Pd(OAc)$_2$. The solvation-corrected relative Gibbs energies and electronic energies (in parentheses) are given in kcal/mol

On the basis of the conformation of the intermediate **DC-7a$_{HOAc}$**, we can also have four possible recycling of catalyst pathways, as illustrated in Fig. 9. These pathways correspond to coordinating of Pd atom with the product, HOAc, and BQ ligand or without ligand, leading to the formation of intermediates **DC-8a$_{HOAc}$**, **DC-8b$_{HOAc}$**, **DC-8c$_{HOAc}$**, and **DC-8d$_{HOAc}$**, respectively. Following steps are coordination of monocationic BQ fragment to the Pd center and the H atom migration. Fig. 10 only shows the Gibbs energy profile of the most favorable pathway for recycling of catalyst, and other pathways are illustrated in supporting information (Fig. S6). The Gibbs energy barriers for recycling of catalyst with the product, HOAc, and BQ ligand are calculated to be 23.2, 23.4, 24.7, and 13.4 kal/mol relative to intermediate **DC-7a$_{HOAc}$**, respectively. It can be seen that the pathway (**DC-8d$_{HOAc}$ → DC-10d$_{HOAc}$**) is more favorable than others (**DC-8a$_{HOAc}$ → DC-10a$_{HOAc}$**, **DC-8b$_{HOAc}$ → DC-10b$_{HOAc}$**, and **DC-8c$_{HOAc}$ → DC-10c$_{HOAc}$**).

In this section, the overall barrier for the (HOAc)$_2$-Pd(BQ)$^{2+}$-catalyzed reaction is calculated to be 28.5 kcal/mol. The coordination of the monocationic BQ fragment to the Pd atom is the rate-determining step along the catalytic cycle.

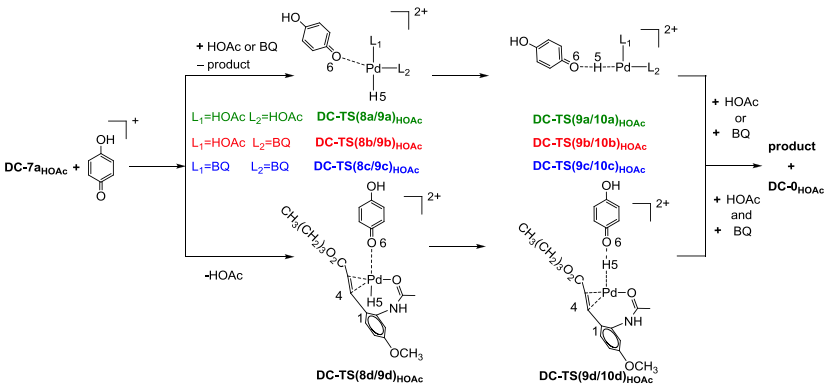

Fig. 9. Proposed pathways for the regeneration of catalyst from DC-7a$_{HOAc}$

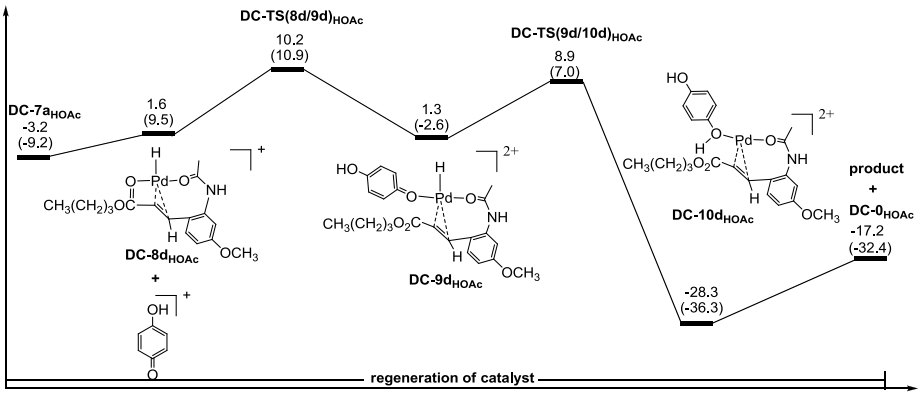

Fig. 10. Gibbs energy profile for the regeneration of catalyst (DC-7a$_{HOAc}$ → DC-0a$_{HOAc}$) in Pd(OAc)$_2$. The solvation-corrected relative Gibbs energies and electronic energies (in parentheses) are given in kcal/mol

3. 3 [Pd(MeCN)$_4$](BF$_4$)$_2$ versus Pd(OAc)$_2$

Combining the results in Figs. 1, 3, 5, 6, 8, and 10, we can map out the completed energy surface for the [Pd(MeCN)$_4$](BF$_4$)$_2$ catalytic system and Pd(OAc)$_2$ catalytic system.

In the case of [Pd(MeCN)$_4$](BF$_4$)$_2$ system, the maximum Gibbs energy barrier is the C−C cross coupling of alkene insertion through transition state **DC-TS(5a/6a)$_{MeCN}$**, with its barrier being 27.2 kcal/mol. In C−H activation, the role of BQ molecule is as a base to provide negative charge to activate the C−H bond. The subsequent alkene insertion and *β*-hydride elimination proceed from **DC-4$_{MeCN}$** to **DC-8a$_{MeCN}$**. The C4 atom of *n*-butyl acrylate attacks the activated C1 atom of 3-methoxyacetanilide; then the transfer of H5 atom forms the Pd−H bond and final cross-coupling product. For recycling of catalyst, monocationic BQ moiety induces the migration of hydrogen again. Through calculation, it is illustrated that MeCN ligand is the most catalytically active ligand than the other ligands in total catalytic cycle. The possible reason is found to be that the Pd metal center and N atom of MeCN ligand maintain the weaker coordination, thereby increasing the activity of the Pd(II) catalytic species and making the Pd-catalyzed C−C cross coupling reaction kinetically and thermodynamically favorable.

In the case of Pd(OAc)$_2$ system, the most favorable one should be the dicationic (HOAc)$_2$Pd(BQ)$^{2+}$ catalyzed mechanism. The corresponding mechanism is the same as what we found for the mechanism of [Pd(MeCN)$_4$](BF$_4$)$_2$ catalyzed reaction. The rate-determining step is proposed to involve the coordination of the monocationic BQ fragment by intermediate **DC-8d$_{HOAc}$** with an activation energy of 28.5 kcal/mol, which differs with the [Pd(MeCN)$_4$](BF$_4$)$_2$ system. In C−H activation, the BQ is as a base to activate the C−H bond. For alkene insertion and *β*-hydride elimination, it proceeds from monocationic **DC-4$_{HOAc}$** to **DC-7a$_{HOAc}$** to form the precursor product. The successive recycling of catalyst occurs. The BQ continuously induces the migration of hydrogen recovering the catalyst, in which the product as ligand coordination with Pd center is the most catalytically active than Pd coordinated with the other ligands. The product ligand has a weaker interaction with Pd metal center than the HOAc and BQ ligands, promoting the recycling of catalyst favorable.

Furthermore, it is found that both [Pd(MeCN)$_4$](BF$_4$)$_2$ and Pd(OAc)$_2$ catalytic systems occur in Pd(II)/Pd(II) catalytic cycle, which is in disagreement with the experimentally proposed Pd(0)/Pd(II) mechanism. After establishing the catalytic cycle, we now analyze the reason why the oxidation states of Pd(II) catalysts [Pd(MeCN)$_4$](BF$_4$)$_2$ and Pd(OAc)$_2$ do not change. The C−H activation from **DC-0$_{MeCN}$** or **DC-0$_{HOAc}$** mainly appear by *σ*-bond metathesis mechanism rather than the oxidative addition mechanism to activate the C−H bond; Then the Pd(II) species (**DC-6a$_{MeCN}$** and D**C-6a$_{HOAc}$**) do not have internal base to extract the H atom, leading to the formation of Pd−H bond, followed by deprotonation through external base, so the oxidation states of Pd metal center have no change.

4 CONCLUSION

In this paper, a systematic theoretical study on the catalytic cycles of the [Pd(MeCN)$_4$](BF$_4$)$_2$ and Pd(OAc)$_2$ systems have been investigated through DFT and the detailed mechanisms are depicted in Scheme 5.

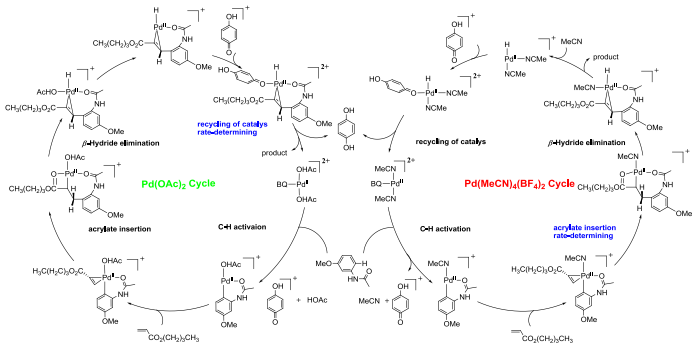

Scheme 5. The most favorable mechanisms for the $[Pd(MeCN)_4](BF_4)_2$ and $Pd(OAc)_2$ systems

In $[Pd(MeCN)_4](BF_4)_2$ system, the rate-determining step is C−C cross coupling of acrylate insertion with the highest Gibbs energy of 27.2 kcal/mol. This system involving dicationic catalytic mechanism contains four sections including C−H activation, acrylate insertion, *β*-hydride elimination, and recycling of catalyst. It is found that the MeCN ligand maintains the weak coordination with the Pd metal center, increasing the activity of the Pd(II) catalytic species and making the Pd-catalyzed aromatic C−H activation reaction kinetically and thermodynamically favorable. The role of BQ is 2-fold, involving as base providing negative charge to activate the C−H bond and helping the catalyst recovery. In $Pd(OAc)_2$ system, the active catalyst is identified as $(HOAc)_2Pd(BQ)^{2+}$ in the presence of HBF_4, BQ, and water. Similar to what we found in the $[Pd(MeCN)_4](BF_4)_2$ system, this system also contains four sections involving C−H activation, acrylate insertion, *β*-hydride elimination, and recycling of catalyst. The rate-determining step is the recycling of catalyst with the highest energy of 28.5 kcal/mol. It is concluded that HOAc ligand is catalytically more active than the BQ ligand. However, in recycling of catalyst section, the product as ligand coordinated with the Pd center is more active as compared to HOAc and BQ ligands, mainly due to the weak coordination with Pd center. And BQ is critical for hydrogen abstraction in the recycling of catalyst. Furthermore, the $[Pd(MeCN)_4](BF_4)_2$ and $Pd(OAc)_2$ catalytic systems both involve a Pd(II)/Pd(II) catalytic cycle mechanism.

This work aims to shed light on the understanding of palladium metal catalyzed Fujiwara-Moritani reaction in detail and help the development of more powerful catalysts in C−H activation/C−C cross-coupling reaction.

REFERENCES

(1) (a) Dick, A. R.; Hull, K. L.; Sanford, M. S. A highly selective catalytic method for the oxidative functionalization of C−H bonds. *J. Am. Chem. Soc*. **2004**, 126, 2300–2301.

(b) Thu, H. Y.; Yu, W. Y.; Che, C. M. Intermolecular amidation of unactivated sp^2 and sp^3 C−H bonds via palladium-catalyzed cascade C−H activation/nitrene insertion. *J. Am. Chem. Soc*. **2006**, 128, 9048–9049.

(c) Kalyani, D.; Dick, A. R.; Anani, W. Q.; Sanford, M. S. A simple catalytic method for the regioselective halogenation of arenes. *Org. Lett*. **2006**, 8, 2523–2526.

(d) Hartwig, J. F. Carbon-heteroatom bond formation catalyzed by organometallic complexes. *Nature* **2008**, 455, 314–322.

(e) Hartwig, J. F. Evolution of C−H bond functionalization from methane to methodology. *J. Am. Chem. Soc*. **2016**, 138, 2–24.

(f) Yang, Y. F.; Chen, G.; Hong, X.; Yu, J. Q.; Houk, K. N. The origins of dramatic differences in five-membered vs six-membered chelation of Pd(II) on efficiency of C(sp^3)−H bond activation. *J. Am. Chem. Soc*. **2017**, 139, 8514–8521.

(g) Shan, C.; Zhu, L.; Qu, L. B.; Bai, R.; Lan, Y. Mechanistic view of Ru-catalyzed C−H bond activation and functionalization: computational advances. *Chem. Soc. Rev.* **2018**, 47, 7552–7576.

(2) (a) Bergman, R. G. Organometallic chemistry: C−H activation. *Nature* **2007**, 446, 391–393.

(b) Lewis, J. C.; Bergman, R. G.; Ellman, J. A. Direct functionalization of nitrogen heterocycles *via* Rh-catalyzed C−H bond activation. *Acc. Chem. Res*. **2008**, 41, 1013–1025.

(3) Chen, X.; Engle, K. M.; Wang, D. H.; Yu, J. Q. Palladium(II)-catalyzed C−H activation/C−C cross-coupling reactions: versatility and practicality. *Angew. Chem. Int. Ed*. **2009**, 48, 5094–5115.

(4) Ackermann, L.; Vicente, R.; Kapdi, A. R. Transition-metal-catalyzed direct arylation of (hetero)arenes by C–H bond cleavage. *Angew. Chem. Int. Ed*.

2009, 48, 9792–9826.

(5) Lyons, T. W.; Sanford, M. S. Palladium-catalyzed ligand-directed C−H functionalization reactions. *Chem. Rev*. **2010**, 110, 1147–1169.

(6) (a) Godula, K.; Sames, D. C−H bond functionalization in complex organic synthesis. *Science* **2006**, 312, 67–72.

(b) Davies, H. M. L.; Manning, J. R. Catalytic C−H functionalization by metal carbenoid and nitrenoid insertion. *Nature* **2008**, 451, 417–424.

(c) Colby, D. A.; Bergman, R. G.; Ellman, J. A. Rhodium-catalyzed C−C bond formation via heteroatom-directed C−H bond activation. *Chem. Rev*. **2010**, 110, 624–655.

(d) Engle, K. M.; Mei, T. S.; Wasa, M.; Yu, J. Q. Weak coordination as a powerful means for developing broadly useful C−H functionalization reactions. *Acc. Chem. Res*. **2012**, 45, 788–802.

(e) Guo, X. X.; Gu, D. W.; Wu, Z.; Zhang, W. Copper-catalyzed C–H functionalization reactions: efficient synthesis of heterocycles. *Chem. Rev*. **2015**, 115, 1622–1651.

(f) Park, Y.; Kim, Y.; Chang, S. Transition metal-catalyzed C−H amination: scope, mechanism, and applications. *Chem. Rev*. **2017**, 117, 9247–9301.

(g) Feng, Z.; Xiao, Y. L; Zhang, X. G. Transition-metal (Cu, Pd, Ni)-catalyzed difluoroalkylation via cross-coupling with difluoroalkyl halides. *Acc. Chem. Res.* **2018**, 51, 2264–2278.

(h) Dai, J.; Lu, D. D.; Ye, T.; Yu, S. Y.; Cheng, X. Experimenting with a Suzuki-Miyaura cross-coupling reaction that demonstrates tolerance toward aldehyde groups to teach undergraduate students the fundamentals of transition-metal catalyzed reactions. *J. Chem. Educ.* **2019**, 96, 2672–2675.

(7) (a) Surry, D. S.; Buchwald, S. L. Biaryl phosphane ligands in palladium-catalyzed amination. *Angew. Chem. Int. Ed*. **2008**, 47, 6338–6361.

(b) Giri, R.; Lan, Y.; Liu, P.; Houk, K. N.; Yu, J. Q. Understanding reactivity and stereoselectivity in palladium-catalyzed diastereoselective sp^3 C–H bond activation: intermediate characterization and computational studies. *J. Am. Chem. Soc*. **2012**, 134, 14118–14126.

(c) Anand, M.; Sunoj, R. B.; Schaefer, H. F. Non-innocent additives in a palladium(II)-catalyzed C–H bond activation reaction: insights into multimetallic active catalysts. *J. Am. Chem. Soc*. **2014**, 136, 5535–5538.

(d) Haines, B. E.; Xu, H. Y.; Verma, P.; Wang, X. C.; Yu, J. Q.; Musaev, D. G. Mechanistic details of Pd(II)-catalyzed C–H iodination with molecular I_2: oxidative addition vs electrophilic cleavage. *J. Am. Chem. Soc*. **2015**, 137, 9022–9031.

(e) He, G.; Wang, B.; Nack, W. A.; Chen, G. Syntheses and transformations of α-amino acids via palladium-catalyzed auxiliary-directed sp^3 C–H functionalization. *Acc. Chem. Res*. **2016**, 49, 635–645.

(f) Yang, Y. F.; Hong, X.; Yu, J. Q.; Houk, K. N. Experimental-computational synergy for selective Pd(II)-catalyzed C–H activation of aryl and alkyl groups. *Acc. Chem. Res*. **2017**, 50, 2853–2860.

(g) Wang, X.; Liu, W. G.; Tung, C. H.; Wu, L. Z.; Cong, H. A monophosphine ligand derived from anthracene photodimer: synthetic applications for palladium-catalyzed coupling reactions. *Org. Lett*. **2019**, 21, 8158–8163.

(8) Moritani, I.; Fujiwara, Y. Aromatic substitution of styrene-palladium chloride complex. *Tetrahedron Lett*. **1967**, 8, 1119–1122.

(9) (a) Wu, J.; Cui, X.; Chen, L.; Jiang, G.; Wu, Y. Palladium-catalyzed alkenylation of quinoline-*N*-oxides via C−H activation under external-oxidant-free conditions. *J. Am. Chem. Soc*. **2009**, 131, 13888–13889.

(b) Cheng, D.; Gallagher, T. Direct and regioselective C−H alkenylation of tetrahydropyrido [1,2-*a*] pyrimidines. *Org. Lett*. **2009**, 11, 2639–2641.

(c) Cho, S. H.; Hwang, S. J.; Chang, S. Palladium-catalyzed C−H functionalization of pyridine *N*-oxides: highly selective alkenylation and direct arylation with unactivated arenes. *J. Am. Chem. Soc*. **2008**, 130, 9254–9256.

(d) Yokota, T.; Tani, M.; Sakaguchi, S.; Ishii, Y. Direct coupling of benzene with olefin catalyzed by $Pd(OAc)_2$ combined with heteropolyoxometalate under dioxygen. *J. Am. Chem. Soc.* **2003**, 125, 1476–1477.

(e) Weissman, H.; Song, X.; Milstein, D. Ru-catalyzed oxidative coupling of arenes with olefines using O_2. *J. Am. Chem. Soc*. **2001**, 123, 337–338.

(10) Mulligan, C. J.; Parker, J. S.; Hii, K. K. (Mimi). Revisiting the mechanism of the Fujiwara-Moritani reaction. *React. Chem. Eng*. **2020**, 5, 1104–1111.

(11) Danton, F.; Najjar, R.; Othman, M.; Lawson, A. M.; Moncol, J.; Ghinet, A.; Rigo, B.; Oulyadi, H.; Da ̈ch, A. Site-selective Pd-catalysed Fujiwara-Moritani type reaction of N,S-heterocyclic systems with olefins. *Adv. Synth. Catal*. **2020**, 362, 1–9.

(12) (a) Liu, X.; Hii, K. K. H. Alternative to benzoquinone for room-temperature Fujiwara-Moritani reactions. *J. Org. Chem.* **2011**, 76, 8022–8026.

(b) Irastorza, A.; Aizpurua, J. M.; Correa, A. Triazole-directed Pd-catalyzed C(sp^2)−H oxygenation of arenes and alkenes. *Org. Lett.* **2016**, 18, 1080–1083.

(c) Lu, W. J.; Jia, C. G.; Kitamura, T.; Fujiwara, Y. Pd-catalyzed selective addition of heteroaromatic C−H bonds to C−C triple bonds under mild conditions. *Org. Lett.* **2000**, 2, 2927–2930.

(d) Gandeepan, P.; Cheng, C. H. Pd-catalyzed π-chelation assisted *ortho*-C–H activation and annulation of allylarenes with internal alkynes. *Org. Lett.* **2013**, 15, 2084–2087.

(13) Nishikata, T.; Lipshutz, B. H. Cationic Pd(II)-catalyzed Fujiwara-Moritani reaction at room temperature in water. *Org. Lett*. **2010**, 12, 1972–1975.

(14) (a) Garcia-Cuadrado, D.; De, P. M.; Braga, A. A.; Maseras, F.; Echavarren, A. M. Proton-abstraction mechanism in the palladium-catalyzed intramolecular arylation: substituent effects. *J. Am. Chem. Soc*. **2007**, 129, 6880–6886.

(b) Davies, D. L.; Donald, S. M. A.; Macgregor, S. A. Computational study of the mechanism of cyclometalation by palladium acetate. *J. Am. Chem. Soc*. **2005**, 127, 13754–13755.

(15) (a) Lapointe, D.; Fagnou, K. Overview of the mechanistic work on the concerted metalation-deprotonation pathway. *Chem. Lett.* **2010**, 39, 1118–1126.

(b) Zhang, L.; Fang, D. C. Catalytic C–H activation/C–C coupling reaction: DFT studies on the mechanism, solvent effect, and role of additive. *J. Org. Chem*. **2013**, 78, 2405–2412.

(16) Frisch, M. J.; Trucks, G. W.; Schlegel, H. B.; Scuseria, G. E.; Robb, M. A.; Cheeseman, J. R.; Scalmani, G.; Barone, V.; Mennucci, B.; Petersson, G. A.; Nakatsuji, H.; Caricato, M.; Li, X.; Hratchian, H. P.; Izmaylov, A. F.; Bloino, J.; Zheng, G.; Sonnenberg, J. L.; Hada, M.; Ehara, M.; Toyota, K.; Fukuda, R.; Hasegawa, J.; Ishida, M.; Nakajima,T.; Honda, Y.; Kitao, O.; Nakai, H.; Vreven, T.; Montgomery, J. A. Jr.; Peralta, J. E.; Ogliaro, F.; Bearpark, M.; Heyd, J. J.; Brothers, E.; Kudin, K. N.; Staroverov, V. N.; Kobayashi, R.; Normand, J.; Raghavachari, K.; Rendell, A.; Burant, J. C.; Iyengar, S. S.; Tomasi, J.; Cossi, M.; Rega, N.; Millam, J. M.; Klene, M.; Knox, J. E.; Cross, J. B.; Bakken, V.; Adamo, C.; Jaramillo, J.; Gomperts, R.; Stratmann, R. E.; Yazyev, O.; Austin, A. J.; Cammi, R.; Pomelli, C.; Ochterski, J. W.; Martin, R. L.; Morokuma, K.; Zakrzewski, V. G.; Voth, G. A.; Salvador, P.; Dannenberg, J. J.; Dapprich, S.; Daniels, A. D.; Farkas, O.; Foresman, J. B.; Ortiz, J. V.; Cioslowski, J.; Fox, D. J. *Gaussian 09, Revision A.02*; Gaussian, Inc.: Wallingford CT **2009**.

(17) Lee, C.; Yang, W.; Parr, R. G. Development of the Colle-Salvetti correlation-energy formula into a functional of the electron density. *Phys. Rev. B* **1988**, 37, 785–789.

(18) Becke, A. D. Density-functional thermochemistry. III. The role of exact exchange. *J. Chem. Phys*. **1993**, 98, 5648–5652.

(19) Stephens, P. J.; Devlin, F. J. *Ab initio* calculation of vibrational absorption and circular dichroism spectra using density functional force fields. *J. Phys. Chem*. **1994**, 98, 11623–11627.

(20) Hariharan, P. C.; Pople, J. A. The influence of polarization functions on molecular orbital hydrogenation energies. *Theor. Chim. Acta* **1973**, 28, 213–222.

(21) (a) Wadt, W. R.; Hay, P. J. *Ab initio* effective core potentials for molecular calculations. Potentials for the transition metal atoms Sc to Hg. *J. Chem. Phys*. **1985**, 82, 270–283.

(b) Hay, P. J.; Wadt, W. R. *Ab initio* effective core potentials for molecular calculations. Potentials for potassium to gold including the outermost core orbitals. *J. Chem. Phys*. **1985**, 82, 299–310.

(22) Ehlers, A. W.; Bohme, M.; Dapprich, S.; Gobbi, A.; Hollwarth, A.; Jonas, V.; Kohler, K. F.; Stegmann, R.; Veldkamp, A.; Frenking, G. A set of f-polarization functions for pseudo-potential basis sets of the transition metals Sc−Cu, Y−Ag and La−Au. *Chem. Phys. Lett.* **1993**, 208, 111–114.

(23) (a) Fukui, K. A formulation of the reaction coordinate. *J. Phys. Chem*. **1970**, 74, 4161–4163.

(b) Fukui, K. The path of chemical reactions the IRC approach. *Acc. Chem. Res*. **1981**, 14, 363–368.

(24) Reed, A. E.; Curtiss, L. A.; Weinhold, F. Intermolecular interactions from a natural bond orbital, donor-acceptor viewpoint. *Chem. Rev*. **1988**, 88, 899–926.

(25) (a) Zhao, Y.; Truhlar, D. G. Density functionals with broad applicability in chemistry. *Acc. Chem. Res*. **2008**, 41, 157–167.

(b) Zhao, Y.; Truhlar, D. G. The M06 suite of density functionals for main group thermochemistry, thermochemical kinetics, noncovalent interactions, excited states, and transition elements: two new functionals and systematic testing of four M06-class functionals and 12 other functionals. *Theor. Chem. Acc*. **2008**, 120, 215–241.

(26) (a) Andrae, D.; Haußermann, U.; Dolg, M.; Stoll, H.; Preuß, H. Energy-adjusted *ab initio* pseudopotentialsfor the second and third row transition elements. *Theor. Chem. Acc*. **1990**, 77, 123–141.

(b) Dolg, M.; Wedig, U.; Preuss, H.; Stoll, H. Energy-adjusted *ab initio* pseudopotentials for the first row transition elements. *J. Chem. Phys*. **1987**, 86, 866–872.

(27) Marenich, A. V.; Cramer, C. J.; Truhlar, D. G. Universal solvation model based on solute electron density and on a continuum model of the solvent defined by the bulk dielectric constant and atomic surface tensions. *J. Phys. Chem. B* **2009**, 113, 6378–6396.